1	Research article
2	Title: Enhanced Adsorption of Methylene Blue by Chemically Modified Materials Derived
3	from Phragmites australis Stems
4	Bui Thi Minh Nguyet <sup>1</sup> , Nguyen Huu Nghi <sup>1</sup> , Nguyen Anh Tien <sup>2</sup> , Dinh Quang Khieu <sup>3</sup> , Ha Danh
5	Duc <sup>1</sup> , and Nguyen Van Hung <sup>1,*</sup>
6	<sup>1</sup> Dong Thap University, Cao Lanh City, 81000, Vietnam
7	<sup>2</sup> Ho Chi Minh City University of Education, Ho Chi Minh City, 700000, Vietnam
8	<sup>3</sup> University of Sciences, Hue University, 530000, Vietnam
9	*Corresponding author: Email: nguyenvanhung@dthu.edu.vn
10	
11	
12	<sup>1</sup> Bui Thi Minh Nguyet, Email: <a href="mailto:btmnguyet@dthu.edu.vn">btmnguyet@dthu.edu.vn</a>
13	<sup>1</sup> Nguyen Huu Nghi, Email: <a href="mailto:nhnghi@dthu.edu.vn">nhnghi@dthu.edu.vn</a>
14	<sup>1</sup> Ha Danh Duc, Email: <a href="mailto:hadanhduc@gmail.com">hadanhduc@gmail.com</a>
15	<sup>1</sup> Nguyen Van Hung, Email: nguyenvanhung@dthu.edu.vn
16	<sup>2</sup> Nguyen Anh Tien, Email: <u>tienna@hcmue.edu.vn</u>
17	<sup>3</sup> Dinh Quang Khieu, Email: <u>dqkhieu@hueuni.edu.vn</u>
18	
19	
20	Highlights
21	• The adsorbent was developed from <i>Phragmites australis</i> biomass.
22	• The physicochemical properties of the adsorbent were analyzed comprehensively.
23	• The adsorption capacity was significantly improved after chemical modification with
24	sodium hydroxide and citric acid.
25	• The adsorption mechanism was investigated in detail.
2.5	
26	

#### **ABSTRACT**

An adsorbent named SA-RPB, derived from raw biomass of *Phragmites australis* and chemically modified with sodium hydroxide and citric acid for adsorbing methylene blue (MB) dye from aqueous solutions, was developed in this study. X-ray diffraction (XRD) results showed that the adsorbent existed mainly as cellulose crystals. The Brunauer–Emmett–Teller (BET) specific surface area analysis indicated that the material formed micropores, each with a capillary diameter of 15.97 nm on average. Fourier-transform infrared spectroscopy (FTIR) results confirmed a significant enhancement of hydroxyl and carboxyl groups on the adsorbent surface after denaturation by citric acid. The adsorption kinetics showed that the pseudo-second-order model precisely simulated the adsorption process. The adsorption isotherm process satisfactorily fitted with the Langmuir model, and the maximum adsorption capacity was 191.49 mg/g at 303 K. The adsorption mechanism analysis showed that the MB adsorption onto the SA-RPB was mainly influenced by electrostatic interactions, hydrogen bonding,  $\pi$ – $\pi$  stacking, and capillary filling of micropores. These findings show that adsorbents developed from raw biomass of *Phragmites australis* modified with NaOH and citric acid can remove MB from aqueous solutions.

**Keywords:** Adsorbent; *Phragmites australis*; Methylene blue; Kinetics; Adsorption mechanism

#### 1. Introduction

Dyes have been extensively used in various industries, such as textile, leather, cosmetics, tanning, paper, food technology, hair coloring, pulp mill, pharmaceuticals, and plastics.<sup>1</sup> The wastewater discharged from these industries causes severe environmental pollution.<sup>2</sup> Among different dyes, methylene blue (MB) is the most widely used for coloring cotton, wood, and silk.<sup>3</sup> MB can damage the eyes of humans and animals. Moreover, MB triggers nausea, vomiting, profuse sweating, and mental instability when it passes through the mouth, and it causes rapid or difficult breathing within short periods after inhaling.<sup>4</sup> Therefore, it is necessary to remove MB from wastewater.

Many advanced techniques have been developed for removing MB. Examples include the Fenton process and combined electrochemical treatments, electrochemical degradation, reverse osmosis, photodecomposition, coagulation/flocculation, membrane processing, oxidative

degradation, electrocoagulation, and carbonaceous nanomaterials.<sup>5–13</sup> Activated carbon is widely and effectively used for removing different dye molecules.<sup>14–16</sup> However, these methods are expensive, owing to poor regeneration. In recent years, considerable efforts have been made in developing sorbents derived from plant materials, such as mango peels, pistachio shell, cladodes of *Opuntia ficus indica*, peach stone, carbonized watermelon, seed fibers, and potato peels.<sup>17–23</sup>

*P. australis* is a type of reed that mainly grows around lakes, rivers, streams, and brackish water worldwide between 10° and 70° northern latitudes.<sup>24</sup> The plant has a high tissue porosity formed by cellulose, hemicellulose, and lignin, which are vital constituents for developing absorbents.<sup>25</sup> *P. australis* naturally and abundantly grows in Viet Nam. In previous studies, low-cost adsorbents were generated from *P. australis* biomass and removed MB.<sup>26,27</sup> In these studies, MB adsorption was conducted using a raw material and a raw material modified with NaOH.<sup>26,27</sup> Plant materials modified with citric acid (CA) show good potential for wastewater treatment.<sup>20,28,29</sup> Cellulose fibrils extracted from *P. australis* treated with NaOH and citric acid may be more effectively modified, enhancing the MB adsorption capacity compared to only treatment with NaOH as described in the previous report.<sup>26</sup> In addition, the effects of environmental parameters on the MB adsorption of raw and modified adsorbents were evaluated.

## 2. Materials and Methods

#### 2.1. Chemicals and materials

Citric acid (HOC(COOH)(CH<sub>2</sub>COOH)<sub>2</sub>,  $\geq$  99.5%), sodium hypophosphite monohydrate (NaH<sub>2</sub>PO<sub>2</sub>.H<sub>2</sub>O,  $\geq$  99.5%), sodium hydroxide (NaOH,  $\geq$  97%), hydrochloric acid (HCl, 37%), sodium chloride (NaCl,  $\geq$  99.5%), and MB (C<sub>16</sub>H<sub>18</sub>N<sub>3</sub>SCl, 99.5%) were purchased from Sigma-Aldrich. The MB was diluted with double-distilled water to a range of 125–300 mg/L. The pH was adjusted using NaOH (0.1 M) and HCl (0.1 M).

Plant samples of *P. australis* gathered from a wetland in Dong Thap province, Vietnam were used for experiments. The plants were cleaned with tap water to remove dirt and other impurities adhered to their surfaces. The plant stems were collected and dried under the sun for four days before being finely ground to approximately 1–2 mm sizes. The obtained biomass was rinsed with distilled water and dried in a vacuum oven at 70 °C to a constant weight. The product was stored in a desiccator and used as raw *P. australis* biomass (RPB).

#### 2.2. Chemical modifications of *P. australis* biomass

RPB (5 g) was added to a 250 mL glass beaker containing 100 mL NaOH (0.5 M). The solution was stirred at 60 °C and 400 rpm using a magnetic bar for 5 h. The biomass was collected and cleaned with distilled water until the pH of the solution was 7.0. The product was then dried in a vacuum oven at 60 °C for 12 h to yield an adsorbent. The biomass modified with NaOH was designated as S-RPB. The S-RPB material was further denatured using a CA solution. Fifty milliliters of CA solution (0.1 M) were added to a 2.0 g S-RPB. NaH<sub>2</sub>PO<sub>2</sub>.H<sub>2</sub>O (2.65 g), used as a catalyst, was added to the solution. The biomass was collected after stirring at 60 °C and 400 rpm using a magnetic bar for 5 h. The biomass was soaked in 50 mL distilled water several times until the pH became 7.0, and it was dried at 60 °C for 12 h, and subsequently, at 140 °C for 3 h. The second modified adsorbent was designated as SA-RPB.

#### 2.3. Characterization of materials

The lignocellulosic composition before and after modification was determined according to the National Renewable Energy Laboratory (NREL) compositional analysis procedure. <sup>30</sup> The C, H, N, S, and O contents of the materials were analyzed using a CHNS-O Elemental Analyzer (Thermo, Flash EA1112, USA). XRD of the products was performed using a MiniFlex 600 diffractometer (Rigaku, Japan) with a radiation source of Cu K $\alpha$ ,  $\lambda$  = 0.15406 nm. The scanned angle (2 $\theta$  values) ranged between 5° and 80° with a step size of 0.01°. The surface morphology of the adsorbents was scanned using the scanning electron microscopy (SEM) technique (FEI-SEM NOVA NanoSEM 450-USA). FTIR spectra of the samples were recorded using an Infrared Affinity-1S spectrophotometer (Shimadzu). BET was determined using N<sub>2</sub> adsorption—desorption isotherms at liquid nitrogen temperature (77 K) using a Quantachrome TriStar 3000 V6.07A adsorption instrument.

## 2.4. Determination of point of zero charge (pH<sub>PZC</sub>)

The pH<sub>PZC</sub> of the adsorbents was determined using the pH drift method described in a previous study.<sup>31</sup> Forty-five milliliters of 0.5 M NaCl with pH values were adjusted from 2 to 12 using 0.1 M NaOH or 0.1 M HCl solution. Distilled water (50 mL) was added, and the pH values were readjusted and considered the initial pH (pH<sub>i</sub>). Next, an adsorbent was added to each flask at 1.0 g/L, incubated at 180 rpm using a magnetic stir bar for 24 h at room temperature (~30 °C). The

differences in the pH ( $\Delta$ pH) values between the initial pH and final pH (pH<sub>f</sub>) ( $\Delta$ pH = pH<sub>i</sub> – pH<sub>f</sub>) were plotted against pH<sub>i</sub>. The points of intersection of the curve with the abscissa at which  $\Delta$ pH is equal to zero were presented as the pH<sub>PZC</sub>.

## 2.5. Adsorption tests

Adsorption tests were performed by adding an adsorbent to a 250 mL glass beaker containing 100 mL MB solution. For the effects of MB concentrations of adsorption, the MB was diluted to 125–300 mg/L. For the effects of the adsorbent on adsorption, SA-RPB (0.4–1.4 g/L) was used. The solution was stirred at 300 rpm, and liquid media were collected from 2 to 105 min. Liquid media samples were centrifuged at 3000 rpm for 5 min to remove solid particles. MB concentrations were measured using an ultraviolet–visual spectrophotometer (Spectro UV–2650, Labomed, USA) at a wavelength of 665 nm. The percent removal (R) and adsorption capacity per unit mass ( $q_t$ ) after a specific contact time (t) were calculated using Eqs. (1) and (2), respectively:

130 
$$R(\%) = \frac{C_0 - C_t}{C_0} \times 100 \tag{1}$$

$$q_{t} = \frac{(C_0 - C_t) \times V}{m} \tag{2}$$

where  $C_0$  (mg/L) and  $C_t$  (mg/L) are the MB concentrations in liquid media at the initial and time t, respectively, and V is the volume of the solution (L).

#### 135 2.5.1. Adsorption kinetics

The adsorption kinetics were fitted to the pseudo-first-order and pseudo-second-order kinetic models. The pseudo-first-order and pseudo-second-order equations are expressed by Eqs. (3) and (4), respectively:<sup>32,22</sup>

139 
$$q_t = q_e (1 - e^{-k_l t}) \tag{3}$$

140 
$$q_t = \frac{q_e^2 k_2 t}{1 + q_e k_2 t} \tag{4}$$

where  $k_I$  (min<sup>-1</sup>) and  $k_2$  (g/mg.min) are the rate constants of the pseudo-first-order and pseudosecond-order, respectively, and t (min) is the contact time.

## 2.5.2. Adsorption isotherms

Four isotherm equations, that is, the Langmuir, Freundlich, Temkin, and Dubinin–Radushkevich equations, were used to fit the experimental equilibrium isotherm data for the MB adsorption on SA-RPB. Adsorption isotherm tests were performed by adding 0.1 g SA-RPB into 100 mL MB (150 mg/L). The initial pH of the MB solution was 6.5, and the controlled temperatures were 30 °C (303 K), 40 °C (313 K), and 50 °C (323 K). The Langmuir model assumes that adsorption is localized on a monolayer, and all adsorption sites on the adsorbent are homogeneous and possess the same adsorption capacity, as expressed by Eq. (5)<sup>35</sup>:

$$q_e = \frac{q_{\text{max}} K_L C_e}{1 + K_I C_e} \tag{5}$$

where  $C_e$  (mg/L) is the equilibrium concentration,  $q_e$  (mg/L) is the amount of adsorbed dye at equilibrium,  $q_{\text{max}}$  (mg/g) is the maximum adsorption capacity, and  $K_L$  (L/mg) is the Langmuir adsorption equilibrium constant. The equilibrium parameter ( $R_L$ ) is a dimensionless constant of the Langmuir isotherm, expressed by Eq. (6)  $^{35}$ :

157 
$$R_L = \frac{1}{1 + K_L C_0} \tag{6}$$

where  $C_0$  is the highest initial solute concentration. The Freundlich isotherm model Freundlich assumes multilayer adsorption processes occur on heterogeneous surfaces, expressed by Eq. (7)<sup>36</sup>:

160 
$$q_e = K_F C_e^{1/n_F}$$
 (7)

where  $K_F$  (mg/g.(L/mg)<sup>1/n</sup>) and n are Freundlich constants related to the adsorption capacity and adsorption intensity, respectively. The adsorbate–adsorbate interactions can cause a decrease in the heat of adsorption of all the molecules in the layer. The Temkin isotherm reflects the effect of the adsorbate interaction on SA-RPB, expressed by Eq. (8)<sup>37</sup>:

$$q_e = (RT/b)\ln(A_T C_e)$$
 (8)

$$B_T = RT/b \tag{9}$$

where  $A_t$  (L/g) and b (g.J/mg.mol) are Temkin's isotherm constants, R (8.314 J/mol.K) is the universal gas constant, and T (K) is the absolute temperature. The Dubinin–Radushkevich isotherm can be applied to examine the characteristics, free energy, and porosity of any adsorbent.<sup>38</sup> The

model has been used to determine the mean free energy of biosorption, expressed by Eqs. (10)–
171 (12):

$$q_e = q_{DR} e^{-K_{DR} \varepsilon^2}$$
 (10)

173 
$$E = 1/\sqrt{2K_{DR}}$$
 (11)

$$\varepsilon = RT \ln(1 + \frac{1}{C_e}) \tag{12}$$

- where  $K_{DR}$  is a constant related to the adsorption energy (mol<sup>2</sup>/kJ<sup>2</sup>),  $q_{DR}$  (mg/g) is the Dubinin–
- Radushkevich isotherm adsorption capacity,  $\varepsilon$  (kJ/mol) is the Polanyi potential, R is the ideal gas
- constant, and T(K) is the temperature. The free energy of adsorption (E) is considered as chemical
- adsorption (E = 8-16 kJ/mol) or physical adsorption (E < 8 kJ/mol).

179

180

## 2.5.3. Adsorption thermodynamics

- The thermodynamic parameters for the MB adsorption onto SA-RPB were evaluated at 303,
- 313, and 323 K. Gibb's free energy change  $(\Delta G^{\circ})$ , enthalpy  $(\Delta H^{\circ})$ , and entropy  $(\Delta S^{\circ})$  were
- calculated using Eqs. (13)–(15).

$$\Delta G^0 = -RT \ln K_t \tag{13}$$

$$\Delta G^0 = \Delta H^0 - T \Delta S^0 \tag{14}$$

The combination of Eqs. (13) and (14) yields Eq. (15):

$$\ln K_L = -\frac{\Delta H^0}{RT} + \frac{\Delta S^0}{R} \tag{15}$$

- where R (8.314 J/mol.K) is the universal gas constant, T (K) is the absolute temperature, and  $K_L$  is
- the Langmuir equilibrium constant. The values of  $\Delta H^{\circ}$  and  $\Delta S^{\circ}$  can be calculated from the slope
- and intercept, respectively, of the linear plot of  $\ln K_L$  versus 1/T.

191

192

## 2.6. Reusability

- After each cycle of batch experiment, the SA-RPB was collected through centrifugation at
- 194 5000 rpm for 10 min. The adsorbent was first washed with absolute ethanol and subsequently rinsed
- with double-distilled water three times. The adsorbent (0.1 mg) was transferred into 100 mL of the
- rinse media, stirred at 300 rpm for 6 hours, and collected through centrifugation at 5000 rpm for
- 197 10 min. The adsorbent was then dried for 24 h at 100 °C until its weight became constant.

#### 3. Results and discussion

#### 3.1. Characterization of materials

The biomass components of *P. australis* are listed in Table 1. The components of the raw RPB were also determined in previous studies <sup>39,40</sup>. The cellulose content significantly increased, whereas hemicellulose and lignin contents comparatively decreased after treatment with NaOH (S-RPB) and NaOH followed with citric acid (SA-RPB) (Table 1). The C content in RBB (46.42%) decreased slightly, whereas the O content (45.82%) and the ratio of O to C increased slightly after treatment with NaOH and citric acid (Table 1). Moreover, the percentages of N, S, Si, K, and Mg significantly decreased after treatment. Acidic and basic solutions are typically used for modifying and/or removing lignin and hemicellulose from plant biomass.<sup>41</sup> The treatment with NaOH resulted in the formation of hydroxyl groups on the S-RPB, which then reacted with citric acid, forming an ester linkage to introduce carboxyl groups into the SA-RPB.<sup>20</sup>

Table 1. Chemical compositions of RPB, S-RPB, and SA-RPB

Parameter	RPB	S-RPB	SA-RPB
Lignocellulosic analysis (dry weight basis), wt%			
Cellulose (%)	43.31	66.32	71.21
Hemicellulose (%)	30.82	15.17	13.28
Lignin (%)	20.37	12.30	9.19
Elemental analysis (dry weight basis), wt%			
C (%)	46.42	45.71	45.23
O (%)	45.82	47.72	48.83
H (%)	5.910	5.610	5.720
N (%)	0.232	0.111	0.021
S (%)	0.313	0.222	0.107
O/C (mol/mol)	0.7403	0.7830	0.8097
Si (%)	1.050	0.021	-
K (%)	0.454	0.284	0.182
Mg (%)	0.601	0.322	0.110

SEM micrograph images of *P. australis* biomass before and after treatment with NaOH and citric acid were captured (Fig. 1). The raw material had a surface composed of fibrous rods (Fig. 1(a)). The surface morphology changed after denaturing with NaOH. The S-RPB sample retained its tubular structure, but the surface became more porous and uneven (Fig. 1(b)). The texture was also rough and irregular after treatment with NaOH, followed by citric acid treatment (Fig. 1(c)). The treatment with citric acid reduces the cavities on the adsorbent surface. Citric acid clogged the carbon surface, which explains the reasons for the reduction in the surface area and pore volume of the adsorbent.<sup>42</sup>

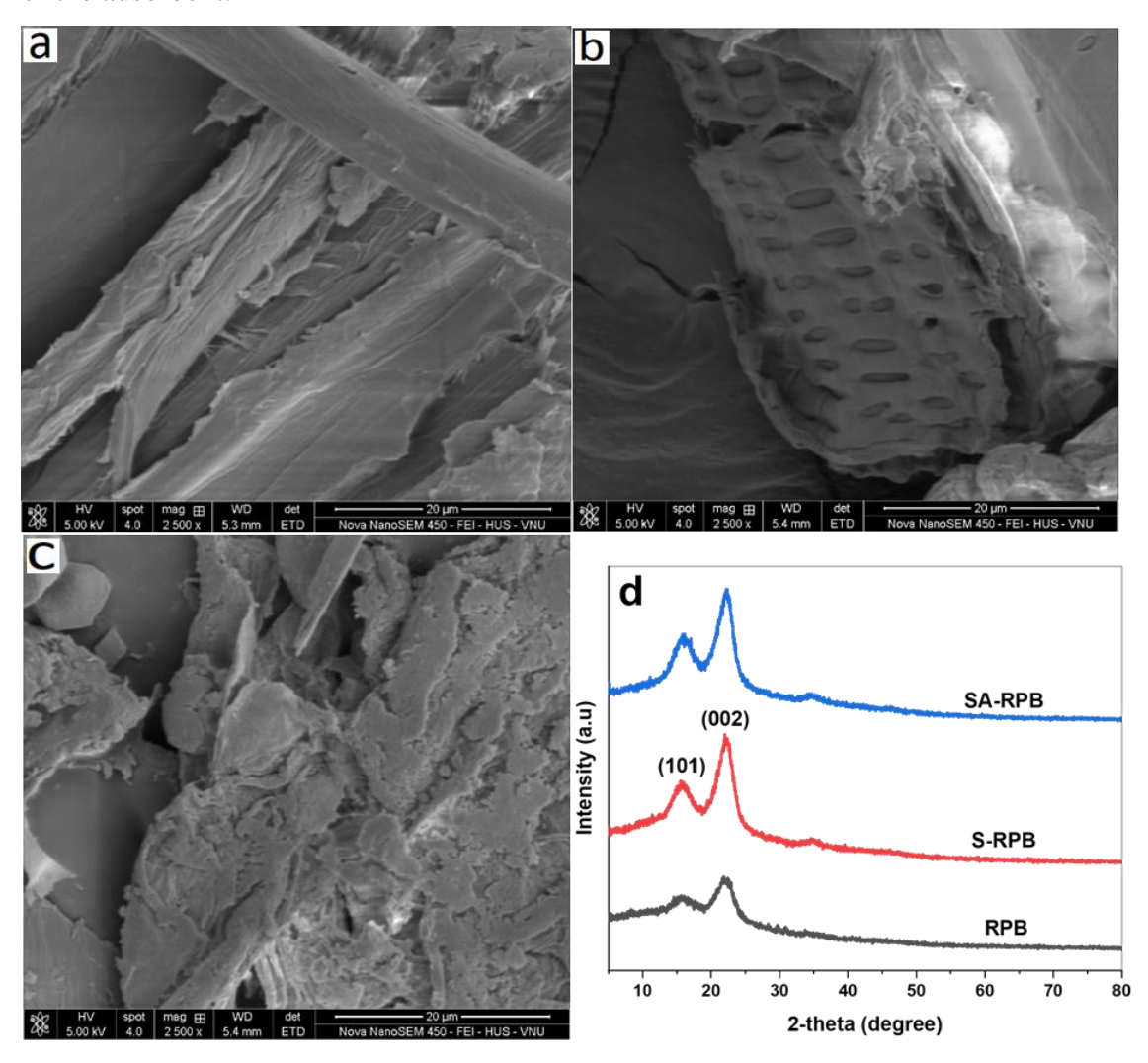


**Fig. 1.** Morphology and crystallization of samples. SEM images of (a) RPB, (b) S-RPB, and (c) SA-RPB; (d) XRD patterns of RPB, S-RPB, and SA-RPB samples.

**Table 2.** Porous textural parameters of RPB, S-RPB, and SA-RPB samples

Sample	Surface area (m²/g)	Pore volume (dm³/g)	Average pore diameter (nm)
RPB	1.01	2.626	16.64
S-RPB	0.87	2.052	16.86
SA-RPB	0.74	1.935	15.97

227

228

229

230

231

232

233

234

235

236

237

238

239

240

241

242

243

244

245

246

247

248

249

225

The crystallographic structures of the RPB, S-RPB, and SA-RPB were analyzed using the XRD technique (Fig. 1(d)). The results indicated that all samples had two diffraction peaks at angles 20 of 15.7° and 22.3°, corresponding to (101) and (002) planes of cellulose crystals. 43 The diffraction intensities were in the order of SA-RPB > S-RPB > RPB (Fig. 1(d)), indicating that NaOH and citric acid enhanced the cellulose crystallinity. Increased crystallization attributed to the partial removal of amorphous polymers (hemicellulose and lignin) from plant structures has also been reported.<sup>26,44</sup> The specific surface area and porous texture of the obtained samples were evaluated using the nitrogen adsorption–desorption isotherms at 77 K (Table 2). The RRB sample had a specific surface area of 1.01 m<sup>2</sup>/g, a common property of raw plant biomasses. <sup>45</sup> The surface areas decreased by 13.9% after treatment with NaOH and 26.7% after treatment with NaOH and citric acid, while the pore volumes decreased by 21.8% and 26.3%. Besides, the average pore diameter slightly decreased after treatment. Citric acid can easily penetrate the pore structure because of its small molecular size, causing the pore block of the adsorbent. 42 These results indicate that the dye adsorption capacity can be improved due to the formation of hydroxyl and carboxyl groups on the surface of P. australis biomass, and the functional groups might play a more important role than the surface area in MB adsorption.

The functional groups on the adsorbent surfaces with differences in intensities of the observed peaks during *P. australis* biomass modification were analyzed using FTIR (Fig. 2). Absorption bands corresponding to functional groups were determined according to Reddy.<sup>46</sup> A broad peak of approximately 3321 cm<sup>-1</sup> corresponded to the stretching vibration of the hydroxyl groups (–OH) for cellulose, hemicellulose, and lignin, whereas the 2918 cm<sup>-1</sup> band indicated the presence of C–H stretching vibrations of methyl and methylene. After the raw material was modified with NaOH and NaOH followed with citric acid, the stretching vibration bands of OH

shifted to 3443 and 3438 cm<sup>-1</sup>, respectively. The band at 1734 cm<sup>-1</sup> could be attributed to the C=O bond stretching of acetyl ester groups in hemicellulose, lignin, or both.

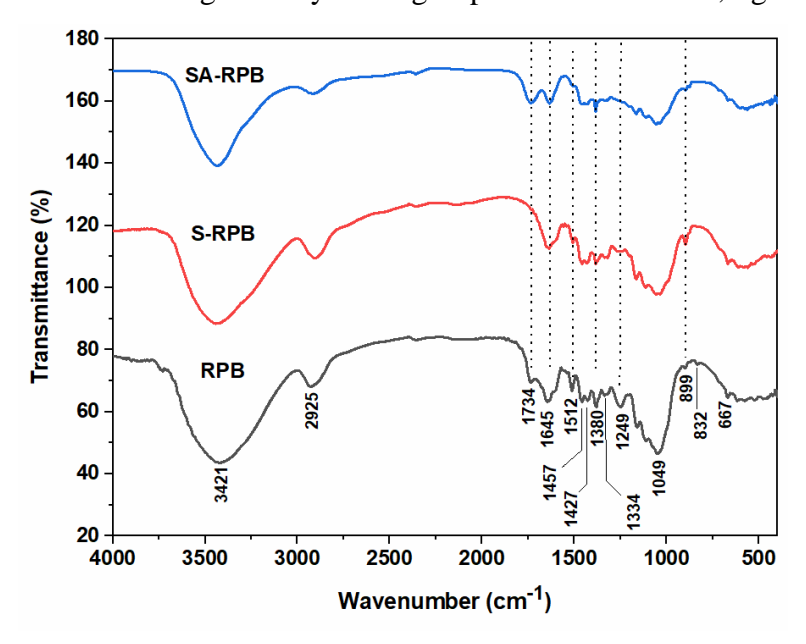


Fig. 2. FTIR spectra of RPB, S-RPB and SA-RPB samples.

This absorption peak was absent from the FTIR spectrum of the S-RPB sample (Fig. 2) after alkaline treatment because of the removal of hemicellulose and lignin through a process called deesterification. Moreover, C=O bond stretching was observed after treatment with NaOH and citric acid, owing to the esterification reaction. The band at 1645 cm<sup>-1</sup> could be attributed to –COO<sup>-</sup> stretching of carboxylate groups with the aromatic ring. The band at approximately 1512 cm<sup>-1</sup> was associated with C=C stretching vibrations in aromatic rings of lignin, whereas the band at 1427 cm<sup>-1</sup> was attributed to the C–H bond deformation of lignin. The peak intensities at 1457 and 1380 cm<sup>-1</sup> reflected C–H symmetric and asymmetric deformations of cellulose, respectively. The appearance of peaks at 1334 and 1327 cm<sup>-1</sup> could be attributed to the –OH bending vibration in C–OH and C1–O vibrations in S derivative vibrations of cellulose, respectively. The signal at 1249 cm<sup>-1</sup> corresponded to the –COO vibration of acetyl groups in hemicellulose and lignin. <sup>20,47</sup> The absorption peaks at 1159 and 1111 cm<sup>-1</sup> were attributed to C–O–C antisymmetric and anhydroglucose ring vibrations, respectively, whereas the band at 1049 cm<sup>-1</sup> corresponded to C–O stretching vibrations of cellulose, hemicellulose, and lignin. <sup>48</sup> A band at 899 cm<sup>-1</sup> corresponds to C–H rocking vibrations of cellulose.

decreased, owing to the removal of lignin. The weak absorption peaks of 832–400 cm<sup>-1</sup> were probably related to C≡H and C=H bending in aromatic rings, C−H bending, and C−O stretching.<sup>40,50</sup> The FTIR results indicated abundant functional groups of −OH, −COOH, and −COO<sup>−</sup> on the adsorbent surfaces.

## 3.2. pH<sub>PZC</sub> determination

The differences in the pH<sub>PZC</sub> of RPB, S-RPB, and SA-RPB are shown in Fig. 3(a). The raw P. australis biomass had a pH<sub>PZC</sub> of 6.72, also obtained in a previous study. <sup>27</sup> The pH<sub>PZC</sub> levels of S-RPB and SA-RPB were 6.17 and 3.10, respectively.

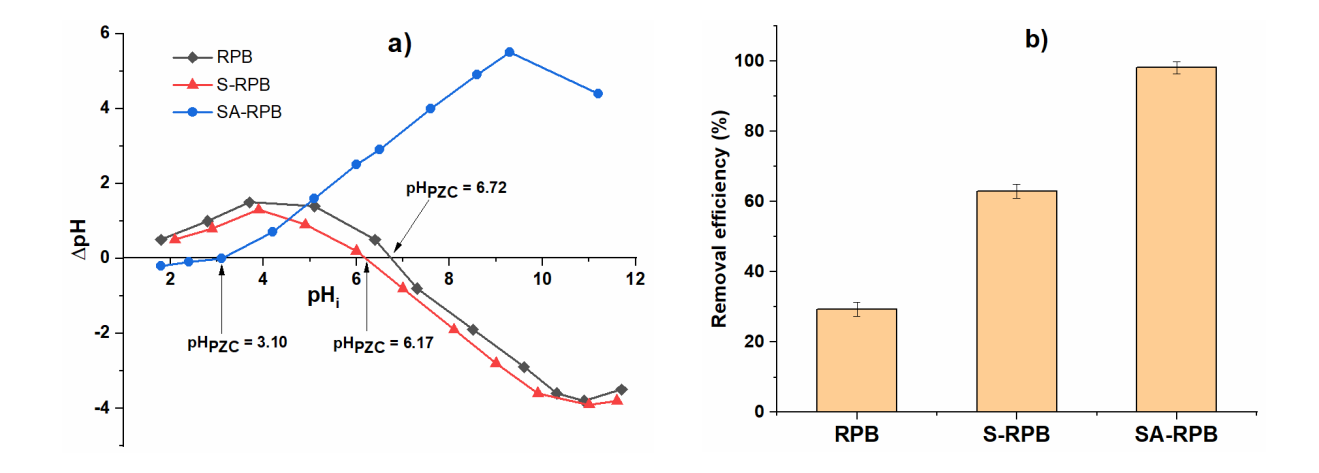


**Fig. 3.** (a) Plots of point of zero charges of RPB, S-RPB, and SA-RPB and (b) percentage removal efficiency values for MB on RPB, S-RPB, and SA-RPB samples.

The pH<sub>PZC</sub> level slightly decreased after treatment with NaOH, possibly because of deesterification and the removal of a part of hemicellulose and lignin.<sup>51</sup> The pH<sub>PZC</sub> value of the SA-RPB was significantly lower than those of RPB and S-RPB, which could be attributed to the esterification reaction of hydroxyl on the raw material surface with the carboxyl group of citric acid to increase the carboxyl group on its surface.<sup>20,52</sup> Absorbents with pH values lower than pH<sub>PZC</sub> absorb compounds with a positive surface charge.<sup>53</sup> The MB dye with a molecular diameter of 0.8 nm<sup>54</sup> was smaller than the pore diameter of SA-RPB (15.97 nm, Table 2); hence, MB could easily penetrate the SA-RPB pore structure. The batch adsorption test results showed that the removal

efficiency of SA-RPB adsorbent was 98.11±1.76%, about 68.8 and 35.1% higher than that of RPB and S-RPB, respectively (Fig. 3(b)). The increase in removal efficiency of SA-RPB was due to the chemical modification of the raw material with NaOH and citric acid. Therefore, SA-RPB was used for other experiments.

# 

#### 3.3. Batch adsorption

#### 3.3.1. Effect of adsorbent dosage

For this experiment, the effects of the adsorbent dose (SA-RPB) on MB adsorption were examined. Fig. 4 shows that an increase in the adsorbent mass from 0.4 to 1.0 g/L improved the MB removal rate because of the increase in the sites available for absorption. However, the adsorption did not statistically increase at adsorbent doses higher than 1.0 g/L. The adsorption tended to an equilibrium when the adsorbent mass reached a particular value, possibly because the available number of MB dye molecules in the solution was insufficient to combine with all effective adsorption sites on the adsorbent.

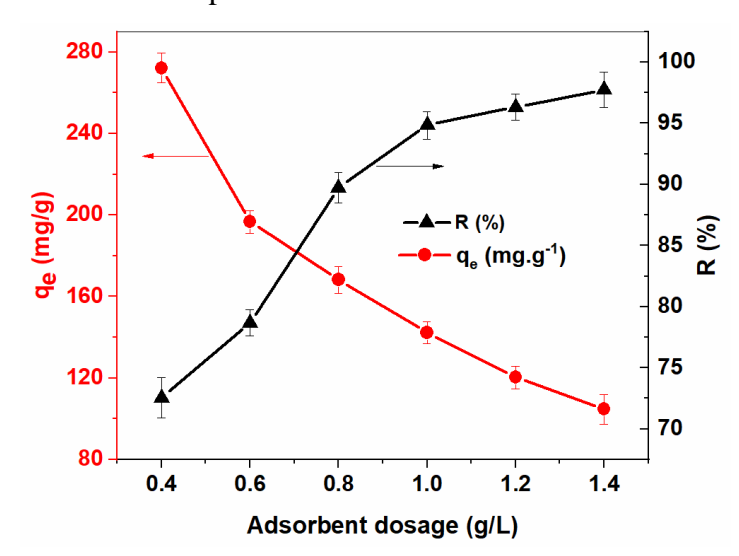


**Fig. 4.** Effect of SA-RPB dosages on equilibrium adsorption capacity ( $q_e$ , mg/g) and removal efficiency of MB (R, %). The tests were conducted for 105 min using 150 mg/L MB at pH of 6.5.

# 

#### 3.3.2. Effects of contact time, temperature, and adsorption kinetics

The effect of contact time on MB removal using the SA-RPB adsorbent is depicted in Fig. 5. The absorption sharply increased within 20 min at the initial stage and then attained equilibrium

after 60 min at all temperatures, after that a maximum removal was attained. About 89.98% of equilibrium adsorption capacity was achieved within 10 min. The fast adsorption at the initial stage may be due to the available vacant active sites of the adsorbent (with functional groups of –OH, –COOH, and –COO<sup>-</sup>) and the higher driving force between MB ions and the surface. However, the adsorption isotherms at three temperatures were not statistically different. This phenomenon is due to the available active sites for adsorption, which previous studies used modified plant materials to remove MB.<sup>55,56</sup> The decrease in the number of vacant sites and the lack of available active sites of the adsorbent decreased the adsorption rate and slowed down the equilibrium.<sup>56</sup>

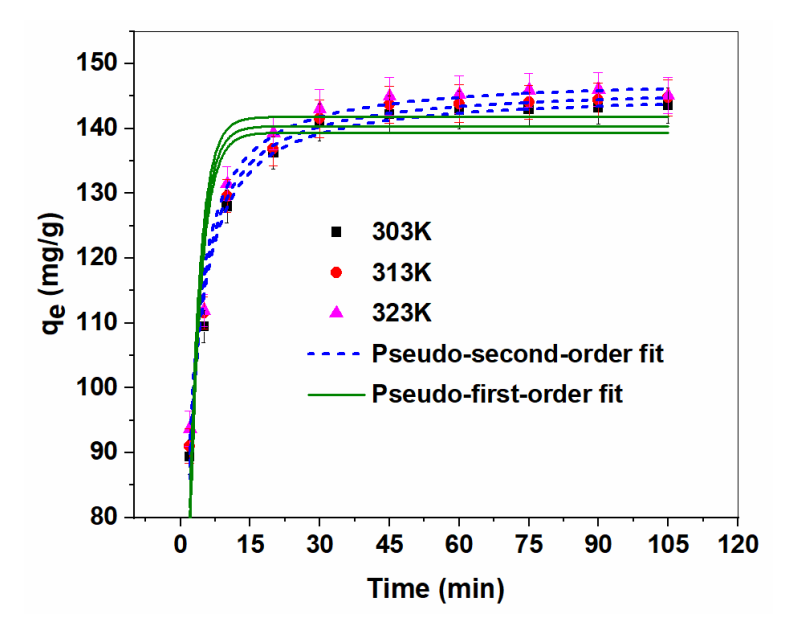


**Fig. 5.** Pseudo-first and pseudo-second-order kinetics for MB adsorption onto SA-RPB at different temperatures. The tests were conducted using 1.0 g/L SA-RPB and 150 mg/L MB at pH of 6.5.

Two kinetic models (pseudo-first-order and pseudo-second-order models) were used to determine the adsorption rate and analyze the kinetic data. The calculated correlation coefficients  $(R^2)$  and other data are listed in Table 3. The  $q_{e,cal}$  and  $q_{e,exp}$  values for each model at different temperatures slightly increased, whereas (and)  $k_1$  and  $k_2$  tended to increase at higher temperatures, indicating that the adsorption kinetics was more rapid at higher temperatures. This shows that the adsorption is the endothermic, in which higher temperature is more favorable for the dye adsorption.

**Table 3.** Kinetic parameters for MB adsorption onto SA-RPB at different temperatures.

Temp. (K)		First-order kinetic model			Second	del			
	q <sub>e,exp</sub> (mg/g)	$k_1$ (min <sup>-1</sup> )	q <sub>e,cal</sub> (mg/g)	$R^2$	$\chi^2$	k <sub>2</sub> (g/mg.min)	q <sub>e,cal</sub> (mg/g)	$R^2$	$\chi^2$
303	143.56	0.4047	139.36	0.807	4.084	0.0049	145.64	0.987	0.340
313	144.75	0.4192	140.35	0.849	3.841	0.0051	146.58	0.989	0.281
323	145.11	0.4275	141.79	0.828	4.241	0.0052	147.93	0.981	0.467

The second-order kinetic model of MB adsorption onto SA-RPB fitted precisely with high correlation coefficients ( $R^2 > 0.98$ ). Moreover, slight differences between the calculated data ( $q_{e,cal}$ ) and experimental data ( $q_{e,exp}$ ) and the low  $\chi^2$  values of the second-order kinetic model indicated the optimum adsorption at the equilibrium of the kinetic model. The pseudo-second-order model better described the experimental data indicating the adsorption highly depended on available active sites than the concentrations of MB. The second-order kinetic model satisfactorily simulates MB adsorption onto modified cellulose fibers of *P. australis*.  $^{26,27}$ 

## 3.3.3. Effects of initial MB concentration and adsorption isotherms

The removal efficiency of MB using SA-RPB depended on the chemical concentration (Fig. 6(a)). The removal rate rapidly increased from 125 to 250 mg/L MB concentrations and gradually increased at higher concentrations. More than 94% MB was absorbed using 125 and 150 mg/L concentrations, and the dye equilibrium adsorption capacity ( $q_e$ ) decreased at higher concentrations (Fig. 6(a)). However, the increase in the initial concentration of MB from 125 to 300 mg/L resulted in the decreases in MB removal from 96.93% to 63.64% at 303 K, from 97.32% to 64.09% at 313 K, and from 97.94% to 64.69% at 324 K (Fig. 6(a)). The lack of available active sites required for the high initial concentration of MB resulted in these reductions. The adsorption isotherms, which revealed the interactive behaviors between the adsorbate and adsorbent at liquid—solid interfaces, were analyzed.

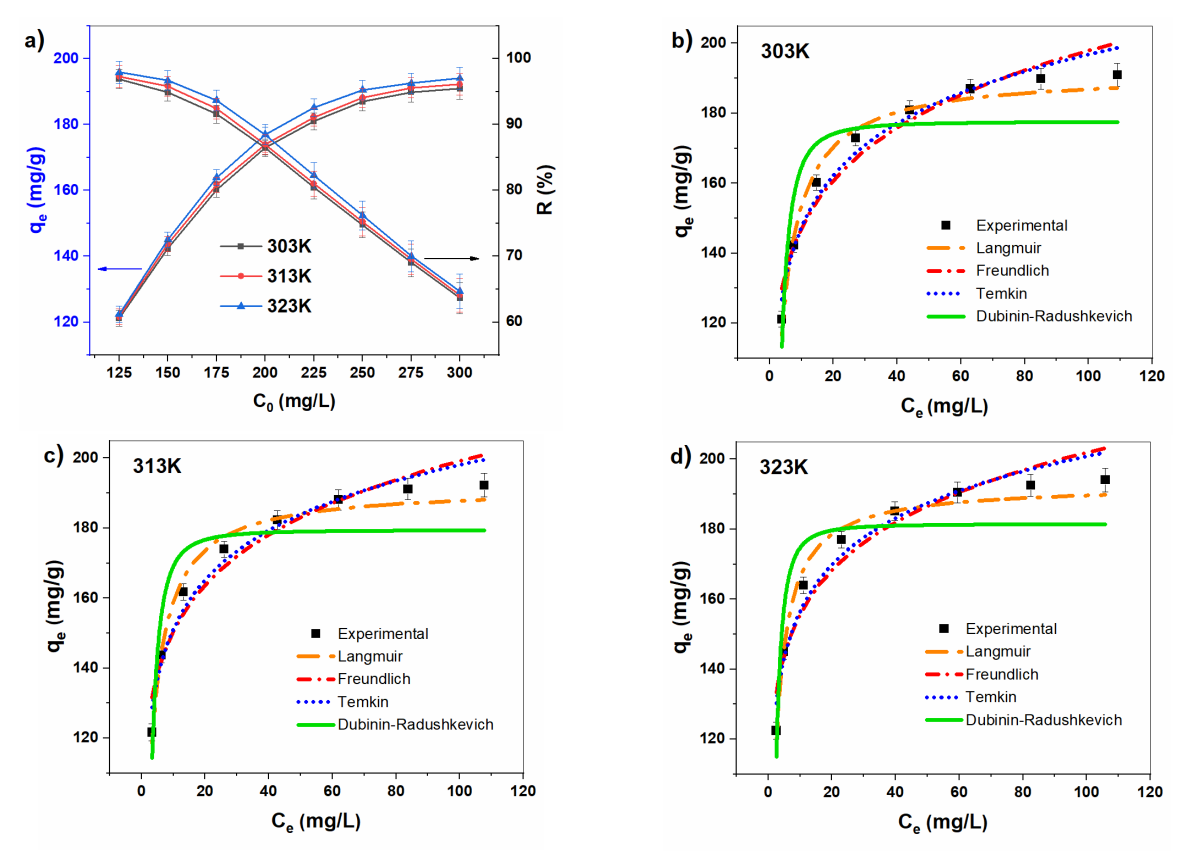


**Fig. 6.** (a) Effect of initial MB concentration on removal efficiency of MB using SA-RPB at different temperatures (the tests were performed using 1.0 g/L SA-RPB and pH of 6.5); (b)–(d) Analyses of MB adsorption isotherm using SA-RPB based on Langmuir, Freundlich, Temkin, and Dubinin–Radushkevich isotherm models at 303, 313, and 323 K. The experiments were conducted using 1.0 g/L SA-RPB at 150 mg/L MB concentration and pH of 6.5.

The Langmuir, Freundlich, Dubinin–Radushkevitch, and Temkin models simulated the MB adsorption onto SA-RPB. The nonlinear plots of the isotherm models at different temperatures are shown in Fig. 6(b)–(d), and their corresponding parameters are listed in Table 4.  $R^2$  and  $\chi^2$  were used as indicators to analyze the adsorption at equilibrium. The Langmuir model yielded the best fit because of its higher  $R^2$  and lower  $\chi^2$  than those of other models. The Langmuir isotherm model showed the homogeneous nature of the adsorbent surface and the monolayer cover of dye molecules formed on the outer surface of the adsorbents under NaOH and citric acid treatment. The  $R_L$  values of the Langmuir isotherm indicated that the fundamental features were higher than 0 and less than 1.0; thus, the adsorption was favorable within the evaluated concentration range.<sup>57</sup>  $R_L$  increased with temperatures, suggesting favorable adsorption of the MB onto the SA-RPB under

the conditions. For the Freundlich model, the 1/n values (Table 4) were within the range of 0.1 < 1/n < 1.0, signifying physisorption mechanism, and the adsorption process was considered favorable, rapid, and effective.<sup>58</sup> The equilibrium models provide insight adsorption mechanism, the surface properties and affinity of the adsorbent.

**Table 4.** Isotherm parameters for MB adsorption onto SA-RPB at different temperatures.

Tomp	~	Langmı	iir isothe	rm			Freundlich	isotherm	1	
Temp. (K)	$q_{\rm e,exp} \ ({ m mg/g})$	$q_{ m max} = ({ m mg/g})$	K <sub>L</sub> (L/mg)	$R_{ m L}$	$R^2(L)$	$\chi^2(L)$	$K_F$ (mg/g. (L/mg) <sup>1/n</sup> )	$n_F$	$R^2(F)$	$\chi^2(F)$
303	190.94	191.49	0.404	0.0082	0.981	0.548	109.15	7.739	0.946	99.505
313	192.27	191.68	0.484	0.0068	0.983	0.482	113.53	8.194	0.946	97.580
323	194.07	192.64	0.629	0.0053	0.983	0.491	119.74	8.815	0.933	96.707
Tomp		Dubinin-Radushkevitch isotherm					Temkin isotherm			
Temp. (K)	$q_{\rm e,exp} \ ({ m mg/g})$	$q_{DR}$ (mg/g)	E (kJ/mol	$K_{DR}$ ) (mol <sup>2</sup> /kJ <sup>2</sup> )	$R^2(DR)$	$\chi^2(DR)$	$A_T(L/mg)$	$B_T$ (J/mol)	$R^2(T)$	$\chi^2(T)$
303	190.94	177.62	0.615	$-1.32 \times 10^{-6}$	0.817	5.135	95.656	21.470	0.970	0.867
313	192.27	179.47	0.716	$-0.97 \times 10^{-6}$	0.846	4.414	163.32	20.414	0.967	0.980
323	194.07	181.48	0.924	$-0.58 \times 10^{-6}$	0.847	4.441	336.91	19.263	0.959	1.244

The obtained adsorbent modified with NaOH and citric acid exhibited effective MB removal with the maximum adsorption capacity of 191.49 mg/g at 150 mg/L MB concentration. This value is higher than those obtained in other studies using modified *P. australis* biomass and other modified plant materials listed in Table 5. For example, Kankılıç *et al.* reported that the maximum adsorption capacity of cellulose microfibrils of *P. australis* modified with NaOH was 54.9 mg/g at 400 mg/L.<sup>58</sup> The treatment with citric acid increased the adsorption ability in this study.

**Table 5.** Comparison of adsorption capacities of different MB adsorbents.

Adsorbent	Temperature (K)	pН	q <sub>max</sub> (mg/g)
P. australis treated with NaOH and citric acid	303	6.5	191.49
P. australis treated with NaOH <sup>26</sup>	298	7.0	54.9
Raw P. australis <sup>58</sup>	298	6.5	22.7
P. australis treated with organic compounds <sup>58</sup>	298	6.5	46.8
Raw Tunisian P. australis <sup>27</sup>	298	8.0	41.2
Peach stones modified with citric acid <sup>20</sup>	303	6.0	178.25
Lawny grass treated with citric acid <sup>28</sup>	298	5.7	301.1
Peanut shell modified with citric acid <sup>29</sup>	303	10.0	120.48
Activated carbon <sup>15</sup>	303	7	81.20

## 3.3.4. Adsorption thermodynamics

Determining thermodynamic parameters is conducted to better understand the effect of temperature on dye adsorption on adsorbents. The Arrhenius equation (Eq. (16)) was used to calculate the effect of temperature on the velocity of a chemical reaction, which is the basis for all predictive expressions of reaction-rate constants.

$$lnk_2 = lnA - \frac{E_a}{RT}$$
 (16)

In Eq. (16), A (g/mg·min) is the pre-exponential factor,  $E_a$  (kJ/mol) is the activation energy of the adsorption, R (8.314 J/mol.K) is the gas constant, and T (K) is the absolute temperature. Plots of  $\ln K_2$  versus 1/T and  $\ln K_L$  versus 1/T were straight lines with  $R^2$  values of 0.99 and 0.98, respectively, from which  $E_a$  and A values were calculated (Table 6). The low values of activation energy (< 42 kJ/mol) obtained in this study indicated a diffusion-controlled process and a physisorption mechanism.<sup>59</sup> The negative values of  $\Delta G^0$  at all temperatures revealed that the adsorption process was feasible and spontaneous. The obtained  $\Delta H^0$  was positive, showing the endothermic nature of adsorption. The positive  $\Delta S^0$  suggested increased randomness of the solid–liquid and adsorption medium interface during adsorption. The positive value of  $\Delta S^0$  also indicates the affinity of the adsorbent for the MB, and some structural changes in adsorbate and adsorbent.<sup>60</sup> **Table 6.** Thermodynamic parameters for MB adsorption onto SA-RPB.

 $E_a$  (kJ/mol)
 A (g/mg.min)
 Temperature (K)
  $\Delta G^0$  (kJ/mol)
  $\Delta H^0$  (kJ/mol)
  $\Delta S^0$  (kJ/mol.K)

 303
 -28.63

 2.242
 0.012
 313
 -30.18
 16.82
 0.155

-31.73

-

3.3.5. Effect of initial pH

The increase in pH from 1.0 to 6.5 significantly increased the adsorption, and the adsorption rates were not significantly changed at a higher pH (Fig. 7). The adsorbent surface becomes more positively charged at low pH, which reduces the attraction between adsorbent and MB. A more negatively charged surface is available when pH increases, facilitating greater MB uptake.<sup>51</sup> The effect of pH on the MB removal efficiency could be attributed to the characteristics of the functional groups on the surface and isoelectric point pH<sub>PZC</sub> of the SA-RPB adsorbent. The

isoelectric point pH<sub>PZC</sub> value of SA-RPB, determined using the drift pH method, was 3.1 (Fig. 3(a)). The hydroxyl (-OH) and carboxyl (-COOH) groups were dominant on the SA-RPB surface, which was deprotonated and became less charged, that is pH<sub>PZC</sub> < 3.1.<sup>61</sup> When the initial pH (pH<sub>in</sub>) was lower than pH<sub>PZC</sub> (3.1), the adsorbent surface was protonated and became more positive.<sup>61</sup> In this case, the SA-RPB surface exhibited an electrostatic repulsion between the SA-RPB surface and the MB-N<sup>+</sup> cation in the solution, leading to poor adsorption efficiency.<sup>62</sup> In contrast, when the pH value was lower than pH<sub>PZC</sub>, the functional groups on the SA-RPB surface were deprotonated and became more negative; this phenomenon induced electrostatic attraction to MB-N<sup>+</sup>, increasing the removal efficiency.<sup>62</sup>

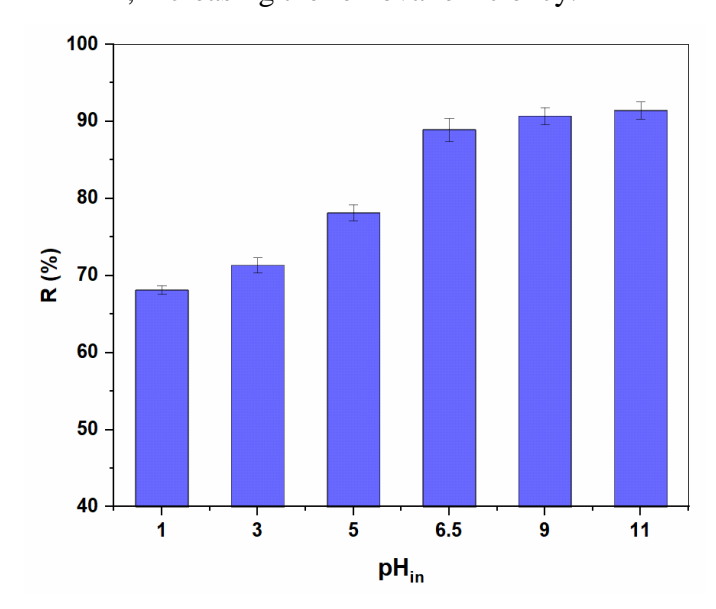


**Fig. 7.** Effect of initial pH value on MB adsorption onto SA-RPB. The tests were performed using 1.0 g/L SA-RPB at 150 mg/L MB concentration.

## 3.3.6. Possible mechanism of MB adsorption onto SA-RPB

Dye adsorption involves interactions between the adsorbent and the adsorbate in the solution. Based on the result ( $\Delta H^o = 16.82 \text{ kJ/mol}$ ), adsorption was mainly induced by electrostatic and/or hydrogen bond forces.<sup>63</sup> At a pH < 3.1 (pH<sub>PZC</sub> of SA-RPB), the protonated adsorbent surface became positively charged (Fig. 3(a)). Therefore, the MB–N<sup>+</sup> adsorption was mainly attributed to the physical interaction caused by capillary diffusion and weak hydrogen bonds. The surface of the negatively charged adsorbent electrostatically interacted with MB–N<sup>+</sup> at pH > 3.1, improving the

adsorption efficiency. The MB adsorption efficiency of the SA-RPB reached the maximum value at the initial pH of the MB solution (6.5); hence, this pH value was selected to evaluate the adsorption mechanism.

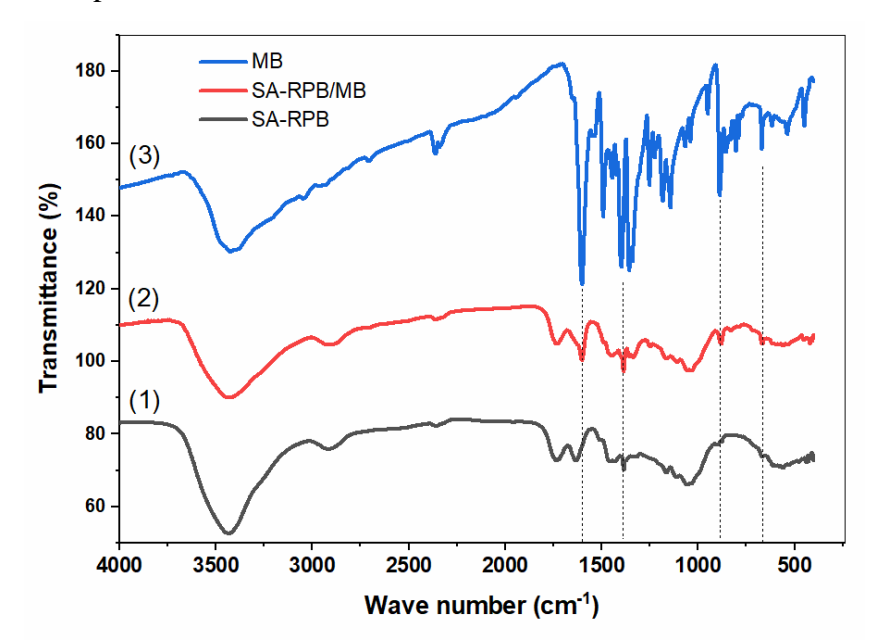


Fig. 8. FTIR spectra of SA-RPB (1) before and (2) after MB adsorption and (3) pure MB.

The FTIR analysis plots showed the spectra of the MB, SA-RPB, and SA-RPB after MB adsorption and were used to describe the adsorption mechanisms. From the spectral peaks (Fig. 8), vibrations were revealed (Table 7). Based on the wavenumbers, it was inferred that pure MB had functional groups, that is, -OH, C=C, C=N, C=N<sup>+</sup>, C-N, C=S, C-S, and C-H.<sup>64,65</sup> The variations in peak positions of the functional groups and the strength of the SA-RPB dye complex indicated MB adsorption onto the SA-RPB surface. The differences in the wavenumbers for C-H deformation in the benzene ring, C-N in the heterocycle and C-N bonds connected with the benzene ring in the MB, C-H aromatic rings, C=C stretching vibrations in aromatic rings, and C-H asymmetric deformation in the SA-RPB and SA-RPB dye complex (Table 7) corresponded to MB attachment to the surface of the adsorbent by  $\pi$ - $\pi$  stacking between the aromatic backbone of the MB and SA-RPB.<sup>50,64</sup> This interaction was evident with absorption peaks of MB and SA-RPB at 1599 and 1506 cm<sup>-1</sup>, respectively, disappearing in the SA-RPB dye complex. Furthermore, the SA-RPB peak at 897 cm<sup>-1</sup> after MB adsorption (Fig. 8), attributed to the bending vibration of C-H in the aromatic ring, increased to a higher intensity than the SA-RPB sample before MB adsorption.

**Table 7.** FTIR spectral characteristics of MB and SA-RPB before and after MB adsorption.

MB		SA-RPB				
Vibration	Wavenumber	Vibration	Wavenumber (cm <sup>-1</sup> )			
	$(cm^{-1})$		Before ads.	After ads.		
O–H or N–H stretching	3424	–OH stretching	3438	3427		
-CH <sub>3</sub> stretching	2939	C-H stretching vibration	2917	2915		
C=N-C group	2360	-COOH stretching vibration	1735	1734		
=N <sup>+</sup> (CH <sub>3</sub> ) <sub>2</sub> stretching	1661	-COO <sup>-</sup> stretching of carboxylate groups with an aromatic ring	1633	1601		
C=N (and C=C) stretching in heterocycle	1599	C=C stretching vibrations in aromatic rings	1506	-		
C-H deformation in benzene ring	1492	C–H deformation in aromatic rings	1456	1489		
C-N in heterocycle	1396	C=C stretching vibrations in aromatic rings	1431	1447		
C-N bonds connected with benzene ring	1356	C-H asymmetric deformation	1384	1385		
N-CH <sub>3</sub> stretching	1340	-OH bending vibration in C-OH	1334	1355		
		C1-O vibrations in S derivatives	1321	1335		
Ar-N deformation vibration	1252		-	1249		
C=S stretching vibration	1183	C-O-C antisymmetric vibrations	1165	1164		
C-S stretching vibration	1142	Anhydroglucose ring vibration	1111	1109		
C-N stretching vibration	1066; 1038	C–O stretching vibration in cellulose, hemicellulose, and lignin	1057; 1035	1056; 1034		
C–H axial deformation in aromataic rings	950–669	C–H rocking vibrations	898	897		
C-S and C-N stretching	616–449	C-H bending in aromatic rings	875-500	875–500		

The peak ranges of 1340–1000 cm<sup>-1</sup> of SA-RPB with oxygen-rich functional groups shifted, suggesting the formation of hydrogen bonds between SA-RPB and MB molecules. The band shifts occurred as N–CH<sub>3</sub> stretching, Ar–N deformation vibration, C=S stretching vibration, and C–S stretching vibration. These phenomena indicated that N in the –N(CH<sub>3</sub>)<sub>2</sub> and Ar–N groups and S in the C=S and C–S groups might have been used as the hydrogen-bonding acceptor and formed intramolecular hydrogen bonding with the hydrogen atom of the –OH and –COOH groups on the adsorbent surface.<sup>64</sup> Hydrogen atoms in the functional groups of SA-RPB could also form hydrogen

bonds with N and S in the functional groups of MB. In addition, the SA-RPB dye complex had a new absorption peak at 1249 cm<sup>-1</sup>, owing to the Ar–N deformation vibration of the MB molecule; this verified MB adsorption onto the SA-RPB surface. Based on the above analysis results, the adsorption efficiency of the MB onto the SA-RPB was attributed to four possible adsorption mechanisms: electrostatic interaction, hydrogen bonding,  $\pi$ – $\pi$  stacking interaction, and filling of pores between the MB and SA-RPB (Fig. 9).

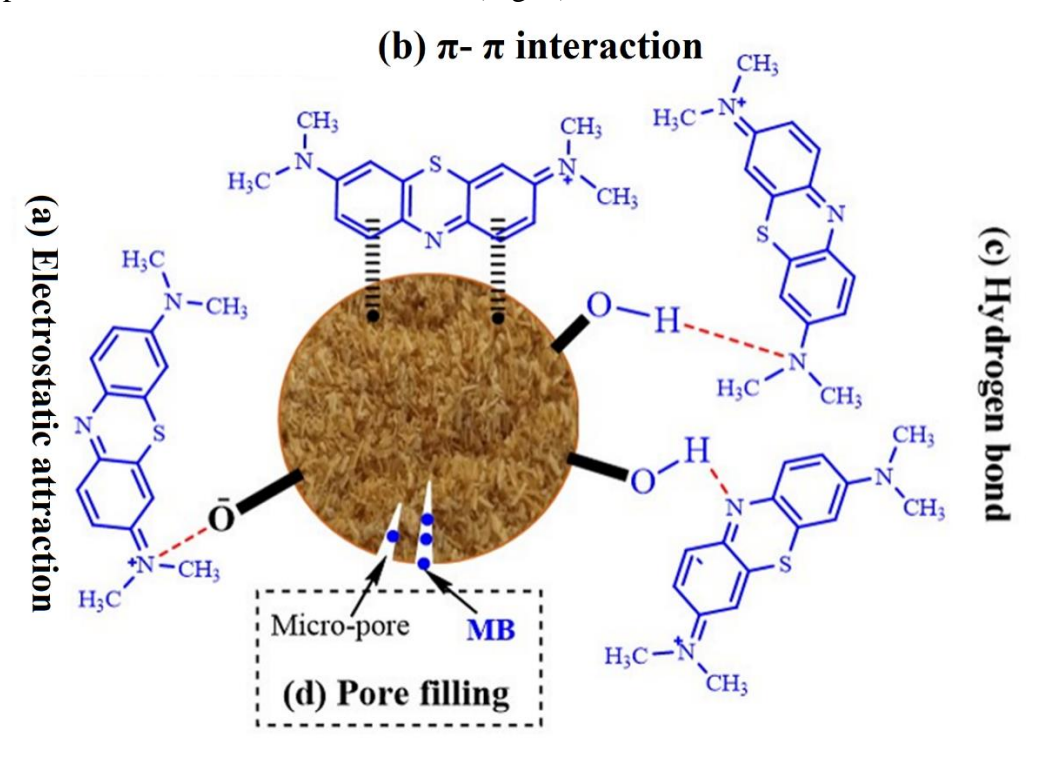
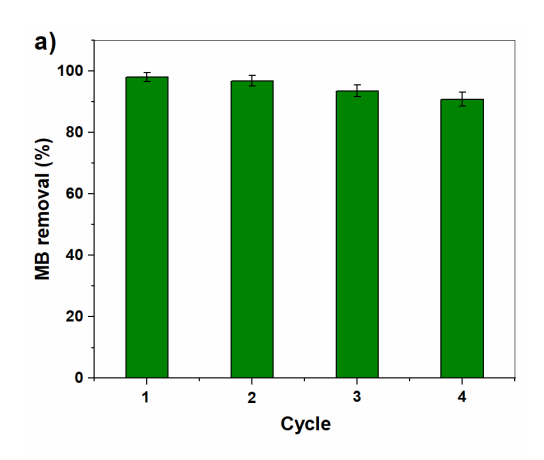
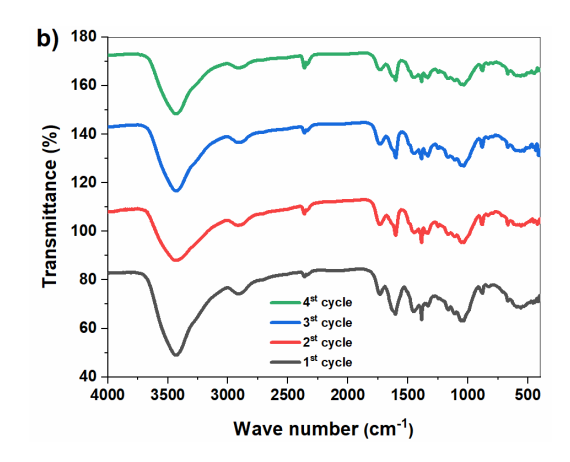


Fig. 9. Possible adsorption mechanism of MB onto SA-RPB.

#### 3.4. Reusability

The reusable efficiency of an adsorbent for wastewater treatment is a critical factor for economic purposes. The regeneration results showed that the adsorption capacity decreased by approximately 7% after four desorption—adsorption cycles compared with the first batch experiment (Fig. 10(a)). Ethanol was used to desorption MB from adsorbents in some previous reports. Additionally, FTIR spectra of adsorbents showed similar spectra after four cycles (Fig. 10(b)), indicating the stability of the adsorbent during the adsorption process. This result suggests that the adsorbent is quite useful for treating real-time industrial effluent.





**Fig. 10.** (a) Removal efficiency of MB onto SA-RPB in successive desorption—adsorption cycles; (b) FTIR spectra of SA-RPB after four desorption—adsorption cycles. The tests were conducted using 1.0 g/L SA-RPB at 150 mg/L MB concentration and pH of 6.5.

## 4. Conclusion

475

476

477

478

479

480

481

482

483

484

485

486

487

488

489

490

491

492

493

494

495

This study demonstrates that chemically modified P. australis biomass can be used as an adsorbent for removing MB dye from aqueous solutions. The batch adsorption test results showed that the material treated with NaOH and citric acid increased the removal compared with the raw material and modified with only NaOH. The initial pH of the solution, the adsorbent dosage, contact time, and initial MB concentrations significantly influenced the adsorption rates of SA-RPB. SEM, FTIR, and BET analysis indicated significant modification in the structure after chemical treatments. Moreover, the calculated adsorption energy indicated that MB adsorption onto SA-RPB occurred through physical interactions at different temperatures when the removal process was endothermic and spontaneous. The maximum adsorption capacity of SA-RPB for MB was 191.49 mg/g, which was slightly decreased after four desorption-adsorption cycles. Four possible adsorption mechanisms, i.e., electrostatic interaction, hydrogen bonding,  $\pi$ - $\pi$  stacking interaction, and filling of pores between the MB and SA-RPB, are attributed to the adsorption. This study shows that a modified material derived from an abundant reed is expected to be highly economical and efficient for removing the synthetic dye in wastewater treatment. For real applications, column experiments are being conducted for possible industrial scale and presented in the future.

497

## Acknowledgements

- This research is supported by the project SPD2020.01.05. The authors are thankful to Dong
- Thap University for providing the instrumental facility and financial support.

500

## 501 Competing interests

- The authors declare that no conflict of interest would prejudice the impartiality of this
- scientific work.

504

#### 505 References

- 506 1. Y. Yao, F. Xu, M. Chen, Z. Xu, Z. Zhu, *Bioresour. Technol.* **2010**, 101(9), 3040–3046.
- **DOI:**10.1016/j.biortech.2009.12.042
- 508 2. L. Meili, P. V. S. Lins, M. T. Costa, R. L. Almeida, A. K. S. Abud, J. I. Soletti, G. L. Dotto,
- E. H. Tanabe, L. Sellaoui, S. H. V. Carvalho, A. Erto, *Prog. Biophys. Mol. Biol.* 2019, 141,
- 510 60–71. **DOI:**10.1016/j.pbiomolbio.2018.07.011
- 3. N. Nasuha, B. H. Hameed, A. T. Din, J. Hazard. Mater. 2010, 175(1-3), 126–132.
- **DOI:**10.1016/j.jhazmat.2009.09.138
- 513 4. M. J. Ahmed, S. K. Dhedan, Fluid Phase Equilibria 2012, 317, 9-14.
- **DOI:**10.1016/j.fluid.2011.12.026
- 515 5. A. Lahkimi, M. A. Oturan, N. Oturan, M. Chaouch, *Environ. Chem. Lett.* **2006**, *5*(1), 35–39.
- **DOI:**10.1007/s10311-006-0058-x
- 517 6. M. Panizza, A. Barbucci, R. Ricotti, G. Cerisola, Sep. Purif. Technol. 2007, 54(3), 382–387.
- **DOI:**10.1016/j.seppur.2006.10.010
- 519 7. S. K. Nataraj, K. M. Hosamani, T. M. Aminabhavi, *Desalination* **2009**, 249(1), 12–17.
- **DOI:**10.1016/j.desal.2009.06.008
- 521 8. F. Gulshan, S. Yanagida, Y. Kameshima, T. Isobe, A. Nakajima, K. Okada, *Water Res.* **2010**,
- 522 44(9), 2876–2884. **DOI:**10.1016/j.watres.2010.01.040
- 523 9. K. L. Yeap, T. T. Teng, B. T. Poh, N. Morad, K. E. Lee, *Chem. Eng. Sci.* **2014**, 243, 305–314.
- **DOI:**10.1016/j.cej.2014.01.004

- 525 10. M. Soniya, G. Muthuraman, *Ind. Eng. Chem.* **2015**, 30, 266–273.
- **DOI:**10.1016/j.jiec.2015.05.032
- 11. M. Khaksar, D. M. Boghaei, M. Amini, Comptes. Rendus. Chimie. 2015, 18(2), 199–203.
- **DOI:**10.1016/j.crci.2014.04.004
- 529 12. M. K. Mbacké, C. Kane, N. O. Diallo, C. M. Diop, F. Chauvet, M. Comtat, T. Tzedakis, J.
- Environ. Chem. Eng. **2016**, 4(4), 4001–4011. **DOI:**10.1016/j.jece.2016.09.002
- 13. W. Ahlawat, N. Kataria, N. Dilbaghi, A. A. Hassan, S. Kumar, K. H. Kim, Environ. Res. 2020,
- 532 *181*, 108904. **DOI:**10.1016/j.envres.2019.108904
- 14. N. Hoc Thang, D. Sy Khang, T. Duy Hai, D. Thi Nga, P. Dinh Tuan, RSC Advances 2021,
- 534 *11*(43), 26563–26570. **DOI:**10.1039/D1RA04672A
- 535 15. M. F. M. Yusop, M. A. Ahmad, N. A. Rosli, M. E. A. Manaf, Arab. J. Chem. 2021, 14(6),
- 536 103122. **DOI:**10.1016/j.arabjc.2021.103122
- 16. F. Marrakchi, M. J. Ahmed, W. A. Khanday, M. Asif, B. H. Hameed, *Int. J. Biol. Macromol.*
- **2017**, 98, 233–239. **DOI:**10.1016/j.ijbiomac.2017.01.119
- 17. A. H. Jawad, N. F. Hanani Mamat, M. Fauzi Abdullah, K. Ismail, *Desalin. Water Treat.* **2016**,
- 540 59, 210–219. **DOI:**10.5004/dwt.2017.0097
- 18. İ. Şentürk and M. Alzein, *Acta Chim. Slov.* **2020**, *67*, 55–69. **DOI:**10.17344/acsi.2019.5195
- 542 19. B. Djobbi, G. L. B. Miled, H. Raddadi and R. B. Hassen, Alzein, Acta Chim. Slov. 2021, 68,
- 543 548-561. DOI: 10.17344/acsi.2020.6248
- 544 20. J. Yan, G. Lan, H. Qiu, C. Chen, Y. Liu, G. Du, J. Zhang, Sep. Sci. Technol. **2018**, 53(11),
- 545 1678–1688. **DOI:**10.1080/01496395.2018.1439064
- 546 21. A. H. Jawad, R. Razuan, J. N. Appaturi, L. D. Wilson, Surf. Interfaces 2019, 16, 76–84.
- **DOI:**10.1016/j.surfin.2019.04.012
- 548 22. N. Sebeia, M. Jabli, A. Ghith, Y. El Ghoul, F. M. Alminderej, Int. J. Biol. Macromol. 2019,
- 549 *121*, 655–665. **DOI:**10.1016/j.ijbiomac.2018.10.070
- 550 23. K. Ben Jeddou, F. Bouaziz, F. Ben Taheur, O. Nouri-Ellouz, R. Ellouz-Ghorbel, S. Ellouz-
- 551 Chaabouni, Water Sci. Technol. **2021**, 83(6), 1384–1398. **DOI:**10.2166/wst.2021.075
- 552 24. A. I. Engloner, *Morphol.* **2009**, 204(5), 331–346. **DOI:**10.1016/j.flora.2008.05.001
- 553 25. T. Březinová, J. Vymazal, *Ecol. Eng.* 2014, *73*, 53–57. **DOI:**10.1016/j.ecoleng.2014.09.022

- 554 26. G. B. Kankılıç, A. Ü. Metin, J. Mol. Liq. **2020**, 312, 113313.
- **DOI:**10.1016/j.molliq.2020.113313
- 556 27. R. Dallel, A. Kesraoui, M. Seffen, J. Environ. Chem. Eng. 2018, 6(6), 7247–7256.
- **DOI:**10.1016/j.jece.2018.10.024
- 558 28. L. Chen, A. Ramadan, L. Lü, W. Shao, F. Luo, J. Chen, J. Chem. Eng. Data. 2011, 56(8),
- 559 3392–3399. **DOI:**10.1021/je200366n
- 560 29. P. Wang, Q. Ma, D. Hu, L. Wang, Water Treat. 2015, 57(22), 10261–10269.
- **DOI:**10.1080/19443994.2015.1033651
- 30. A. Sluiter, B. Hames, R. Ruiz, C. Scarlata, J. Sluiter, D. Templeton, D. Crocker, National
- Renewable Energy Laboratory Golden Co., **2008**.
- 31. M. Danish, T. Ahmad, S. Majeed, M. Ahmad, L. Ziyang, Z. Pin, S. M. Shakeel
- Iqubal *Bioresour*. *Technol*. *Rep.* **2018**, *3*, 127–137. **DOI:**10.1016/j.biteb.2018.07.007
- 566 32. S. Lagergren, *Handlingar Band*, **189**8, 24(4), 1–39.
- 33. Y. S. Ho, G. McKay, Process Biochem. 1999, 34, 451-465. DOI:10.1016/S0032-
- 568 9592(98)00112-5
- 34. L. Mouni, L. Belkhiri, J.-C. Bollinger, A. Bouzaza, A. Assadi, A. Tirri, F. Dahmoune, K.
- 570 Madani, H. Reminie, *Appl. Clay Sci.* **2018**, *153*, 38–45. **DOI:**10.1016/j.clay.2017.11.034
- 571 35. K. R. Hall, L. C. Eagleton, A. Acrivos, T. Vermeulen, *Ind. Eng. Chem. Fundam.* **1966**, *5*(2),
- 572 212–223. **DOI:**10.1021/i160018a011
- 573 36. H. M. Freundlich, J. Phys. Chem. A. **1906**, 57, 385–470.
- 574 37. M. J. Temkin, V. Pyzhev, URSS. 1940, 12, 217–225.
- 575 38. M. M. Dubinin, L. V. Radushkevich, *Proceedings of the Academy of Sciences of the USSR*.
- **1947**, *55*, 331–337.
- 39. H. Zhao, H. Yan, C. Zhang, X. Liu, Y. Xue, Y. Qiao, Y. Tian, S. Qin, Evid. Based Complement
- 578 Alternat. Med. **2011**, 408973. **DOI:**10.1155/2011/408973
- 579 40. A. El Shahawy, G. Heikal, *Ecol. Eng.* **2018**, *122*, 207–218.
- **DOI:**10.1016/j.ecoleng.2018.08.004
- 581 41. D. D. Q. Melo, V. D. O. S. Neto, F. C. D. F. Barros, G. S. C. Raulino, C. B. Vidal, R. F. do
- Nascimento, J. Appl. Polym. Sci. **2016**, 133(15), 43286. **DOI:**10.1002/app.43286

- 583 42. J. P. Chen, S. Wu, K.-H. Chong, *Carbon.* **2003**, *41*(10), 1979–1986. **DOI:**10.1016/S0008-
- 584 6223(03)00197-0
- 585 43. P. Lu, Y. L. Hsieh, ACS Appl. Mater. Interfaces. 2010, 2(8), 2413-2420.
- **DOI:**10.1021/am1004128
- 587 44. D.-Y. Kim, B.-M. Lee, D. H. Koo, P.-H. Kang, J.-P. Jeun, *Cellulose* **2016**, *23*(5), 3039–3049.
- 588 **DOI:**10.1007/s10570-016-1037-4
- 589 45. A. Barakat, C. Mayer-Laigle, A. Solhy, R. A. D. Arancon, H. de Vries, R. Luque, RSC Adv.
- **2014**, 4(89), 48109–48127. DOI **DOI:**10.1039/C4RA07568D
- 591 46. K. O. Reddy, B. R. Guduri, A. V. Rajulu, J. Appl. Polym. Sci. 2009, 114(1), 603–611.
- **DOI:**10.1002/app.30584
- 593 47. C. Uma Maheswari, K. Obi Reddy, E. Muzenda, B. R. Guduri, A. Varada Rajulu, *Biomass*
- *and Bioenergy* **2012**, *46*, 555–563. **DOI:**10.1016/j.biombioe.2012.06.039
- 595 48. C. Pappas, P. A. Tarantilis, I. Daliani, T. Mavromustakos, M. Polissiou, *Ultrason. Sonochem.*
- **2002**, *9*(1), 19–23. **DOI:**10.1016/S1350-4177(01)00095-5
- 597 49. A. Alemdar, M. Sain, *Bioresour Technol.* **2008**, 99(6), 1664–1671.
- **DOI:**10.1016/j.biortech.2007.04.029
- 599 50. L. Hevira, Zilfa, Rahmayeni, J. O. Ighalo, H. Aziz, R. Zein, J. Ind. Eng. Chem. 2021, 97, 188–
- 600 199. **DOI:**10.1016/j.jiec.2021.01.028
- 51. D. H. K. Reddy, Y. Harinath, K. Seshaiah, A. V. R. Reddy, Chem. Eng. Sci. 2010, 162, 626–
- 602 634. **DOI:**10.1016/j.cej.2010.06.010
- 52. H. Nazir, M. Salman, M. Athar, U. Farooq, A. Wahab, M. Akram, Water Air Soil Pollut. 2019,
- 604 230, 303. **DOI:**10.1007/s11270-019-4360-1
- 53. E. C. Lima, B. Royer, J. C. Vaghetti, N. M. Simon, B. M. da Cunha, F. A. Pavan, J. Hazard.
- 606 *Mater.* **2008**, *155*(3), 536–550. **DOI:**10.1016/j.jhazmat.2007.11.101
- 607 54. B. H. Hameed, A. A. Ahmad, J. Hazard. Mater. 2009, 164(2-3), 870–875.
- **DOI:**10.1016/j.jhazmat.2008.08.084
- 609 55. M. M. Abd El- Latif, A. M. Ibrahim, Desalin. Water Treat. 2012, 6(1-3), 252-268.
- **DOI:**10.5004/dwt.2009.501
- 611 56. D. Pathania, S. Sharma, P. Singh, Arab. J. Chem. 2017, 10(1), S1445-S1451.
- **DOI:**10.1016/j.arabjc.2013.04.021

- 613 57. V. Vilar, C. Botelho, R. Boaventura, J. Hazard. Mater. 2007, 147(1-2), 120–132.
- **DOI:**10.1016/j.jhazmat.2006.12.055
- 615 58. G. B. Kankılıç, A. Ü. Metin, İ. Tüzün, Ecol. Eng. **2016**, 86, 85–94.
- **DOI:**10.1016/j.ecoleng.2015.10.024
- 59. M. Al-Ghouti, M. A. Khraisheh, M. N. Ahmad, S. Allen, J. Colloid Interface Sci. 2005, 287(1),
- 618 6–13. **DOI:**10.1016/j.jcis.2005.02.002
- 619 60. Y. Bulut, H. Aydın, *Desalination* **2006**, *194*(1-3), 259-267. **DOI:**10.1016/j.desal.2005.10.032
- 620 61. T. Maneerung, J. Liew, Y. Dai, S. Kawi, C. Chong, C. H. Wang, Bioresour. Technol. 2016,
- 621 200, 350–359. **DOI:**10.1016/j.biortech.2015.10.047
- 622 62. X. Liu, C. He, X. Yu, Y. Bai, L. Ye, B. Wang, L. Zhang, Powder Technol. 2018, 326, 181–
- 623 189. **DOI:**10.1016/j.powtec.2017.12.034
- 624 63. J. Mattson, H. Mark, Marcel Dekker, Ins., New York. 1971.
- 625 64. J. Gong, J. Liu, Z. Jiang, X. Wen, E. Mijowska, T. Tang, X. Chen, J. Colloid Interface Sci.
- **2015**, *445*, 195–204. **DOI:**10.1016/j.jcis.2014.12.078
- 627 65. M. Danish, T. Ahmad, S. Majeed, M. Ahmad, L. Ziyang, Z. Pin, S. S. M. Iqubal, *Bioresour*.
- 628 *Technol. Rep.* **2018**, *3*, 127–137. **DOI:**10.1016/j.biteb.2018.07.007
- 629 66. T. Benhalima, H. Ferfera-Harrar, Int. J. Biol. Macromol. 2019, 132, 126–141.
- **DOI:**10.1016/j.ijbiomac.2019.03.164
- 631 67. S. Lapwanit, T. Sooksimuang, T. Trakulsujaritchok, J. Environ. Chem. Eng. 2018, 6(5), 6221–
- 632 6230. **DOI:**10.1016/j.jece.2018.09.050